Soils and Rocks

An International Journal of Geotechnical and Geoenvironmental Engineering

www.soilsandrocks.com

ISSN 1980-9743
ISSN-e 2675-5475

# Numerical simulation of the size effect on rock particle crushing behavior considering microscopic heterogeneous bond strength characteristics

Jiong Qiu[1], Du-min Kuang[1#], Meng-bo Wang[1], Long Chen[1], Cheng Peng[1], Zhao-bo Song[1]

Article

**Keywords**
Particle crushing
Discrete element method
Weibull distribution
Size effect

**Abstract**

The heterogeneity of microelement strength of rock particle materials is one of the main factors that cause the size effect of the rock particle crushing behavior. In this paper, a numerical model of rock particles that considering the characteristic of microscopic heterogeneous bond strength was established by using Weibull distribution theory through discrete element method. Single particle crushing experiments were carried out on five groups of rock particles and numerical particles with different particle sizes (6-21 mm), the crushing strength and failure modes of rock particles and numerical particles with different sizes were obtained. The results shows that the proposed numerical model can effectively reproduce the size effect of rock particle crushing behavior. The particle crushing strength data are satisfied the Weibull statistical model and have obvious size effect. The particle failure modes can be divided into three different failure types: "brittle" failure, "quasi brittle" failure, and "ductile" failure. As the particle size increase, the particle failure mode changes from "ductile" failure to "brittle" failure. Finally, a microscopic damage function model of particle crushing was established based on the numerical simulation results, which explained the microscopic mechanism of the size effect of particle crushing behavior. This study not only helps to improve the stability of engineering materials, but also optimizes engineering design and construction, and promotes related technological innovation.

## 1. Introduction

Rock particle material has the characteristics of good compressibility, small deformation, and high shear strength, so it is widely used in railway, highway, tunnel, and other filling projects (Wang et al., 2015). However, when the external force exceeds the bearing limit of rock particles, uneven settlement caused by particle breakage can cause incalculable losses to the normal use of engineering buildings (Chen et al., 2017; Feng et al., 2016). In addition, the change of gradation and interaction force caused by particle crushing, will also have a great influence on the engineering mechanical properties of rockfill dams (Zhou et al., 2019). Therefore, understanding the crushing behavior of rock particle materials is of great important for the safety of engineering construction.

At present, research on the mechanical properties of rock particle materials mainly focuses on experimental studies such as uniaxial compression experiments, triaxial compression experiments, triaxial shear experiments, and cyclic load experiments. Song et al. (2022) obtained the compaction deformation relationship of the lateral limit crushed coal rock body by studying the compaction characteristics of crushed coal gangue with different gradation. Yokura et al. (2015) concluded the plastic work calculated from the results of stress-strain relationship and relative crushing degree (*Br*) by conducted compression tests on sandy soil. Zhu et al. (2009) conducted uniaxial compression experiments based on the numerical simulation method, obtained the curve relationship between the compressive strength and size of basalt, established a Weibull distribution model of mechanical properties from a microscopic perspective. Zhang et al. (2011) and Shi et al. (2020) clarified the differences between different strength parameters inside rock particle materials through triaxial compression experiments. Guo et al. (1997) provided a detailed discussion to the effect of particle breakage inside the specimen on the overall shear strength based on triaxial shear experiments. Li et al. (2016) proposed a peak shear velocity strength model for rock particle materials based on the shear strength characteristics of rock particle materials under different shear velocity conditions. Although the particle crushing characteristics and their correlation with the mechanical behavior can be elucidated through the

[#]Corresponding author. E-mail address: kuangdumin@xtu.edu.cn
[1]Xiangtan University, College of Civil Engineering, Xiangtan, China.

Submitted on September 9, 2023; Final Acceptance on October 28, 2024; Discussion open until May, 31, 2025.

Editor: Renato P. Cunha

https://doi.org/10.28927/SR.2025.009723

aforementioned experimental approaches, but they cannot provide a reasonable explanation for their crushing behavior at a microscopic scale. Therefore, various microscopic testing approaches such as X-ray micro-computed tomography (Zheng et al., 2019) and CT scanning technology (Du, 2014) have been adopted to capture the microscopic crushing behavior of crushable particles. However, these approaches have not been widely applied due to the constraints of costly experimental equipment.

The Discrete Element Method (DEM) is a numerical simulation method for discontinuous deformation proposed by Cundall (1971). Typically, there are two DEM-based approaches for simulating the particle crushing, the fragment substitution method (Tavares & Chagas, 2021) and the aggregate method (Cil et al., 2020). The former mainly replaces the original particles that have already crushed by using non cohesive elementary balls. When using this method for particle crushing simulation, it is necessary to manually set particle crushing criteria and fragment replacement modes, which makes the particle crushing mode significantly different from the actual particle. In contrast, the aggregate method provides superior capabilities in simulating the multi-scale crushing behavior of individual particles by modeling individual crushable particles as a collection of bonded elementary balls. For example, Rabiei et al. (2023) analyzed the influence of rock particle sample size on compressive elastic modulus, crack initiation, and crack damage stress limit based on the aggregate method. Zhou et al. (2019) simulated the random compressive strength of rockfill particles by introducing subcritical crack propagation theory into the aggregate particle DEM model.

As is well known, the size effect of rock particle crushing behavior is mainly caused by the heterogeneity of microelement strength and the shape of particles (Jo et al., 2011). Therefore, how to reasonably reflect the heterogeneity of microelement strength and the shape of the particles are the key to whether the numerical model can correctly reproduce the size effect of rock particle crushing behavior. Barbosa et al. (2022) provided a detailed discussion on the influence of soil particles with different shapes on their crushing behavior based on the discrete element method. Zhou et al. (2017) conducted numerical simulations of single particle compression tests on five groups of different particle sizes and shapes of rockfill particles based on discontinuous deformation analysis methods, analyzed the influence of particle interface unit strength on particle fragmentation. Zhang & Huang (2022) introduced inhomogeneous stiffness and strength properties obeying a Gaussian distribution into the numerical model based on bonded particle method (BPM), reproduced the size effect of particle crushing strength. Zhao & Liu (2020) by using the advantages of the random field theory in characterizing the spatial variation and uncertainty of microscopic material properties, analyzed the detailed fracturing mechanism of rock mass. Although the above research has thoroughly analyzed the influence of heterogeneity in micro element strength and particle shape on this phenomenon, but there is no reasonable explanation for the particle crushing behavior from a microscopic perspective.

Based on the previous researchers results, this paper introduces non-homogeneous bond strength parameters into irregular aggregate particle model by discrete element method, so as to establish a numerical model of rock particles considering the characteristics of microscopic heterogeneous bond strength, reproduced the size effect of rock particle crushing behavior. The relationship between particle size, crushing strength, and crushing mode was discussed in detail. Finally, a microscopic damage function relationship model for particle breakage damage was established based on the numerical simulation results. Explained the microscopic mechanism of size effect in rock particle crushing behavior. This study has a certain guiding role in improving the stability of engineering materials, optimizing engineering design and construction.

## 2. Single particle crushing experiment and discrete element modeling

### 2.1 Experimental materials and scheme

The basalt rockfill material in Yunnan Province of China was selected as the experimental material in this study. All basalt particles are divided into different particle size groups of 6-9 mm, 9-12 mm, 12-15 mm, 15-18 mm, 18-21 mm, and with 35 particles in each group, as shown in Figure 1. In addition, Table 1 shows their Poisson ratio, Internal friction angle, Volume density, and Porosity, which were determined through uniaxial compression experiment, triaxial compression experiment, and other geotechnical experiments.

The uniaxial compression experiment of basalt particles was carried out by universal material testing machine, as shown in Figure 2. The left side is the loading system, and the right side is the control system. The loading system mainly consists of top platen, bottom platen, and pressure sensors. The top and bottom plates are made of steel plates with a diameter of 100 mm and a thickness of 20 mm, used for loading granular materials. Pressure sensors are used to measure the pressure value of the granular materials during the compression process. The control system mainly consists of a hydraulic controller and an operation monitoring system. During the loading process, the hydraulic controller is used to control the speed and displacement of the top plate, and the operation monitoring system is used to monitor and record the force displacement curve and the peak crushing force of particle crushing during the testing process. In this experiment, the basalt particles were placed at the center of the bottom platen, and the top platen was moved downward at a uniform speed of 1 mm/min until the particles were crushed.

**Table 1.** Physical properties of basalt particles with different particle sizes.

| Particle sizes (mm) | Poisson ratio | Internal friction angle (°) | Volume density (g/cm$^3$) | Porosity (%) |
|---|---|---|---|---|
| 6-9 | 0.213 | 53.132 | 2.838 | 0.531 |
| 9-12 | 0.221 | 53.574 | 2.939 | 0.874 |
| 12-15 | 0.232 | 55.339 | 2.841 | 1.089 |
| 15-18 | 0.254 | 56.132 | 2.842 | 1.111 |
| 18-21 | 0.267 | 56.651 | 2.845 | 1.134 |

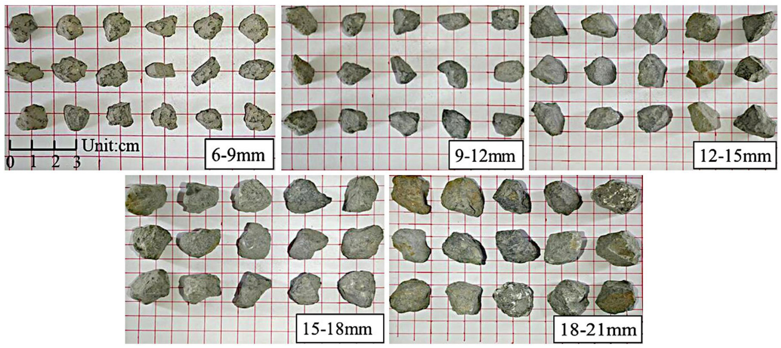


**Figure 1.** Part of basalt particles with different size groups.

## 2.2 Constitutive of linear parallel bond model

Aggregate method is one of the most widely used methods to simulate particle breakage in discrete element method (Zhao & Liu, 2020; Zhou et al., 2017). In the numerical simulations, the rock particle is generally constructed as a particle aggregate, which consists of many rigid balls of finite size that are cemented by linear parallel bonds. The linear parallel bonds are assumed to be a cylinder that transmits both contact force and contact moment, as shown in Figure 3.

The parallel-bond force $\overline{F}$ is resolved into a normal and shear force, and the parallel-bond moment $\overline{M}$ is resolved into a twisting and bending moment, they can be calculated by:

$$\overline{F}=\overline{F}_n\hat{n}_c+\overline{F}_s \tag{1}$$

$$\overline{M}=\overline{M}_t\hat{n}_c+\overline{M}_b \tag{2}$$

where $\hat{n}_c$ is the unit-normal vector. $\overline{F}_n$ and $\overline{F}_s$ are the normal and shear force. $\overline{M}_t$ and $\overline{M}_b$ are the twisting and bending moment. And during the process of loading, they can be calculated by the following:

$$\overline{F}_n=\overline{F}_n+\overline{k}_n\overline{A}\Delta\delta_n \tag{3}$$

$$\overline{F}_s=\overline{F}_s-\overline{k}_s\overline{A}\Delta\delta_s \tag{4}$$

$$\overline{M}_t=\overline{M}_t-\overline{k}_s\overline{J}\Delta\theta_t \tag{5}$$

$$\overline{M}_b=\overline{M}_b-\overline{k}_n\overline{I}\Delta\theta_b \tag{6}$$

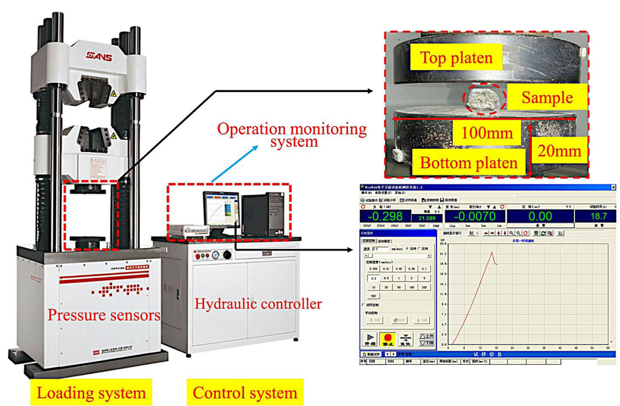


**Figure 2.** Universal material testing machine.

where $\overline{k}_n$ and $\overline{k}_s$ are the normal and shear stiffness, $\Delta\delta_n$ and $\Delta\delta_s$ are the relative normal-displacement increment and the relative shear-displacement increment within a certain calculation time step, $\Delta\theta$ and $\Delta\theta_b$ are the relative twist-rotation increment and the relative bend-rotation increment within a certain calculation time step. $\overline{A}$ is the cross-sectional area, $\overline{J}$ and $\overline{I}$ are the moment and the polar moment of inertia of the parallel bond cross section, respectively, and they can be calculated by:

$$\overline{A}=\pi\overline{R}^2 \tag{7}$$

$$\overline{J}=\frac{1}{2}\pi\overline{R}^4 \tag{8}$$

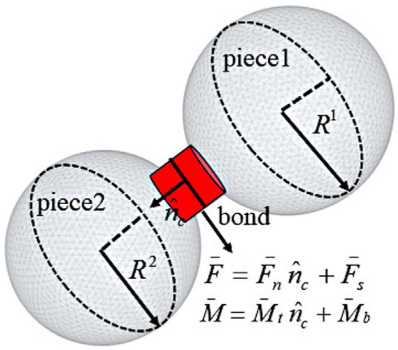


**Figure 3.** Diagram of linear parallel bond.

$$\bar{I}=\frac{1}{2}\pi\bar{R}^4 \tag{9}$$

$$\bar{R}=\begin{cases}\min\left(R^{(1)},R^{(2)}\right), \text{ball-ball}\\ R^{(1)}, \text{ ball-facet}\end{cases} \tag{10}$$

During the calculation process, the stress of the parallel-bond is divided into tensile stress $\bar{\sigma}$ and shear stress $\bar{\tau}$, which are calculated by:

$$\bar{\sigma}=\frac{\bar{F}_n}{\bar{A}}+\bar{\beta}\frac{\left|\bar{M}_b\right|\bar{R}}{\bar{I}} \tag{11}$$

$$\bar{\tau}=\frac{\bar{F}_s}{\bar{A}}+\bar{\beta}\frac{\left|\bar{M}_t\right|\bar{R}}{\bar{J}} \tag{12}$$

where $\bar{\beta}\in[0,1]$ is the moment-contribution factor. If the tensile-strength limit $\bar{\sigma}_c$ and the shear-strength limit $\bar{\tau}_c$ are exceeded ($\bar{\sigma}>\bar{\sigma}_c, \bar{\tau}>\bar{\tau}_c$), then the bond will be destroyed.

### 2.3 Establishment of numerical model

To ensure the numerical particles are closer to the actual particles, The irregular convex polyhedral generated by random simulation technology (Zhou et al., 2009, 2017; Matsumoto & Nishimura, 1998; Ma et al., 2011) are used as boundary walls for numerically aggregated particles, and then the rigid sphericity is randomly placed in the boundary wall. As stated by Fu et al. (2017), in order to reasonably reproduce the crushing behavior of particles, the number of elementary balls in the aggregates needs to be 700-1000. Therefore, the radius of the rigid sphere is set to 0.03 mm in this experiment, which can ensure that the number of elementary balls in each aggregate are more than 2500. The rigid spheres are bonded by linear parallel bond model, and a certain time step is run to eliminate the overlap between the rigid spheres until the particles reach equilibrium, finally the boundary wall is removed. Considering that the strength of each microelement of rock material has the heterogeneity characteristics of Weibull distribution (Li, 1995; Krajcinovic & Silva, 1982; Xu & Wei, 2002). Therefore, set the value of tensile strength and the cohesion that representing the bond strength between the elementary balls in the aggregate particles to obey the Weibull distribution, as shown in Figure 4. The Weibull distribution formula is derived from the Weibull empirical formula (McDowell & Bolton, 1998), as follows:

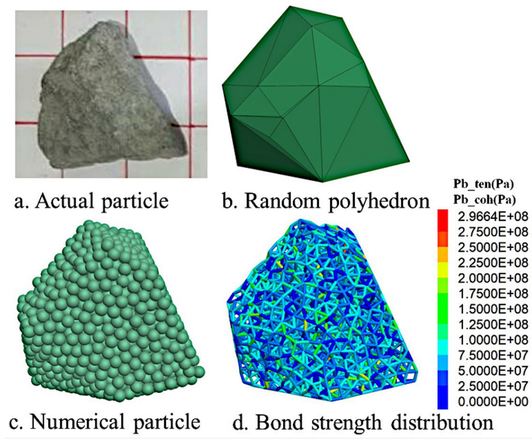


**Figure 4.** Actual sample and numerical sample.

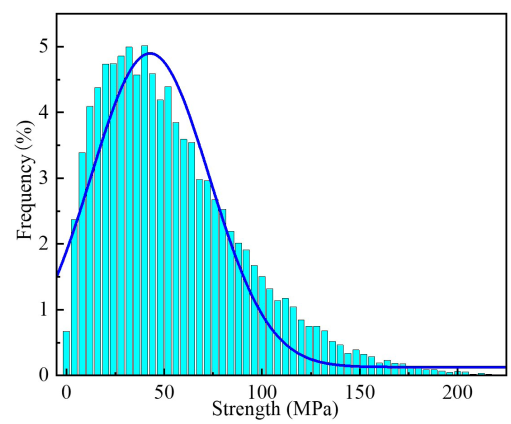


**Figure 5.** Frequency distribution of bond strength.

$$\delta=\Phi*\left[-\ln(1-U(0,1))\right]^{\frac{1}{t}} \tag{13}$$

where $\Phi$ is the mean value of bond strength, $t$ is a constant value. They are obtained by debugging the numerical simulation results to match the experimental results. Finally, the $\Phi$ of the tensile strength and cementation cohesion of this experiment are set to 8.1 MPa, $t$ is set to 1.5. $U$ is a random value that obeys the uniform distribution in [0,1]. Figure 5 shows the frequency distribution of bond strength between the elementary balls.

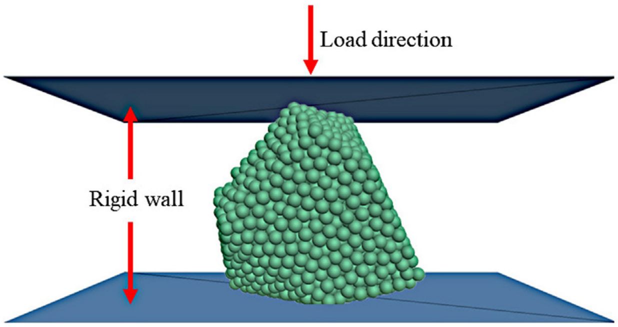


**Figure 6.** Schematic diagram of numerical sample loading.

In the loading process, two rigid numerical walls are employed to simulate the rigid loading platens in physical experiment. as shown in Figure 6. Before compressing, the numerical sample is placed on the bottom rigid wall directing vertically. The quasi-static loading is simulated by moving the top rigid wall to the specimen at a certain speed (1 mm/min) until the specimen is crushed. During the loading process, the contact force and position of the top rigid wall are monitored in real time. And, in order to further study the microscopic breakage process of particle, the occurrence of particle crushing is also obtained by real-time monitoring.

### 2.4 Calibration of the model

The microscopic parameters of the numerical model are calibrated by matching the force-displacement curve of the basalt particle crushing experiment, as shown in Figure 7. The final selected microscopic parameters are shown in Table 2.

## 3. Results and discussion

### 3.1 Statistical analysis of particle crushing strength

According to the description of Jaeger (1967), the crushing strength of particles when they are compressive by two parallel platens can be expressed as:

$$\sigma=\frac{F}{d^2} \tag{14}$$

where $\sigma$ is the crushing strength of the particles. F is the peak force of the particles. d is the particle diameter, which is equal to the distance between two loading platens prior to compression. Experimental studies have shown that (Zhou et al., 2019; Zhang & Huang, 2022), the survival probability $P_s$ of rock particles with different size under uniaxial compression obeys Weibull distribution:

$$P_s = \exp\left[-\left(\frac{d}{d_0}\right)^3\left(\frac{\sigma}{\sigma_0}\right)^m\right] \tag{15}$$

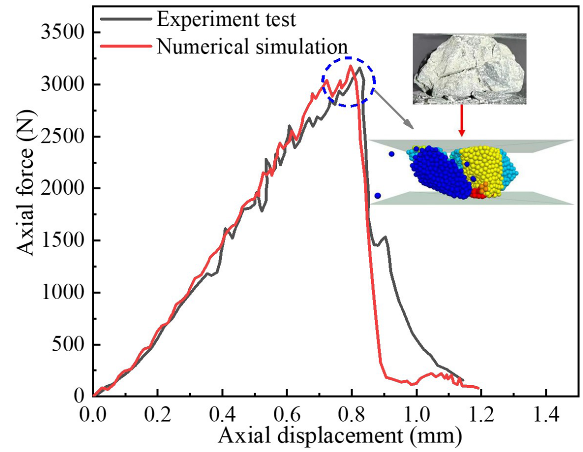


**Figure 7.** Comparison between simulation result and experiment result.

where $d_0$ is the reference particle diameter, $\sigma_0$ is the characteristic crushing strength when 37% of the particles survive, m is the Weibull modulus.

In the particle crushing experiment, the particle survival probability $P_s$ can be calculated by the following:

$$P_s = \frac{i}{N_i} \tag{16}$$

where i is the number of surviving particles at the applied tensile stress, $N_i$ is the total number of particles.

Substituting $d = d_0$ into Equation 15, and taking quadratic natural logarithm on both sides, we can get:

$$\ln\left(\ln\left(\frac{1}{P_s}\right)\right)=m\ln\left(\frac{\sigma}{\sigma_0}\right) \tag{17}$$

The Equation 17 shows that the $\sigma$ and the $P_s$ have a linear relationship in the double logarithmic coordinates, and the slope of the straight line is the size of the *m*.

According to Equations 15-17, Figure 8 shows the survival probability plot and the normalized survival probability plot of experimental test particles and numerical simulation particles with different particle sizes in this study, the normalized survival probability plot embedded in the survival probability plot. From the diagram, it can be seen that the crushing strength of all rock particles and numerical particles with different sizes are satisfied the Weibull statistical model well. Table 3 presents the results of experimental tests and numerical simulations for the characteristic crushing strength and Weibull modulus. It can be seen that with the increase of particle size, the characteristic crushing strength and Weibull modulus of the experiment test and numerical simulation are decreasing, showing a significant size effect. In addition, from Figure 8 and Table 3, it can be also found

**Table 2.** Microscopic parameters of numerical samples.

| | Parameter | Symbol | Value |
|---|---|---|---|
| Linear parallel bond model | Effective modulus | $E^*$ (Pa) | $3.8\times10^9$ |
| | Normal stiffness | $\bar{k}_n$(N/m) | $1\times10^{10}$ |
| | Shear stiffness | $\bar{k}_s$ (N/m) | $8\times10^9$ |
| | Stiffness ratio | $\bar{k}_n/\bar{k}_s$ | 1.25 |
| | Tensile strength | $\bar{\sigma}_c$ (Pa) | Weibull distribution |
| | Cohesion | $\bar{c}$ (Pa) | Weibull distribution |
| | Friction angle | $\Phi$ (°) | 55 |
| | Friction coefficient | $\mu^*$ | 0.1 |
| Modeling Parameters | Density | $P$ (kg/m$^3$) | 2650 |
| | Damping coefficient | $\beta$ | 0.7 |
| | Rigid radius | $R$ (mm) | 0.03 |

Legend: see List of Symbols and abbreviations.

**Table 3.** The results of $\sigma_0$ and $m$.

| Particle size (mm) | Experiment test | | Numerical simulation | |
|---|---|---|---|---|
| | $\sigma_0$ (MPa) | $m$ | $\sigma_0$(MPa) | $m$ |
| 6-9 | 36.90 | 3.09 | 39.82 | 3.15 |
| 9-12 | 33.68 | 2.93 | 35.28 | 3.04 |
| 12-15 | 28.94 | 2.92 | 29.90 | 3.01 |
| 15-18 | 25.27 | 2.84 | 26.19 | 2.91 |
| 18-21 | 24.28 | 2.74 | 24.46 | 2.79 |

that the experiment test results, and numerical simulation results are quite close, indicating that the numerical model proposed in this paper is reasonable.

### 3.2 Influence of particle size on particle crushing mode

Due to the complex morphology of rock particles and the heterogeneity of microelement strength, a variety of overall failure modes will occur during uniaxial compression (Zhang et al., 2022; Ma et al., 2017). In this study, according to the force-displacement curve pattern and the different forms in the crushing process of the real particle and numerical particle, the particles are roughly divided into three different failure modes, as shown in Figure 9.

Figure 9a Mode I, at the beginning of loading, the edges and corners of the particle surface will be broken first, and the force-displacement curve of particle crushing will have multiple peaks at this time. Then, with the increase of load force, a main crack appears in the middle of the particle, and the force-displacement curve drops sharply. Finally, the particles are break into two fragments of similar size, showing a typical “brittle failure” characteristic.

Figure 9b Mode II, at the initial stage of loading, the surface of the particles is slightly break, and the axial force also fluctuates slightly. When the load force continues to increase, multiple microcracks will appear on the surface of the particles, and the whole particles begin to damage. With the rapid expansion of the main crack, the axial force drops greatly. Finally, the secondary crack and the main crack run through the sample synchronously, making the particles break into multiple fragments, showing a “quasi brittle failure” characteristic.

Figure 9c Mode III, at the beginning of loading, there will be a certain grinding and crushing on the surface of the particles, accompanied by a small drop of the axial force. When the load force continues to increase, multiple cracks in the particles simultaneously expand and penetrate the sample, making the axial force fluctuating increase. Finally, the particles are break into multiple fragments, showing a certain degree of “ductile failure” characteristic.

Figure 10 shows the statistical frequency of different failure modes in each rock particle size group. From the Figure 10, with the increase of particle size, the Statistical frequency of Mode I is gradually increasing, and the statistical frequency of Mode II and Mode III is gradually decreasing. It is means that, the failure mode of particles gradually changes from “ductile” failure mode to “brittle” failure mode with the particle size increase.

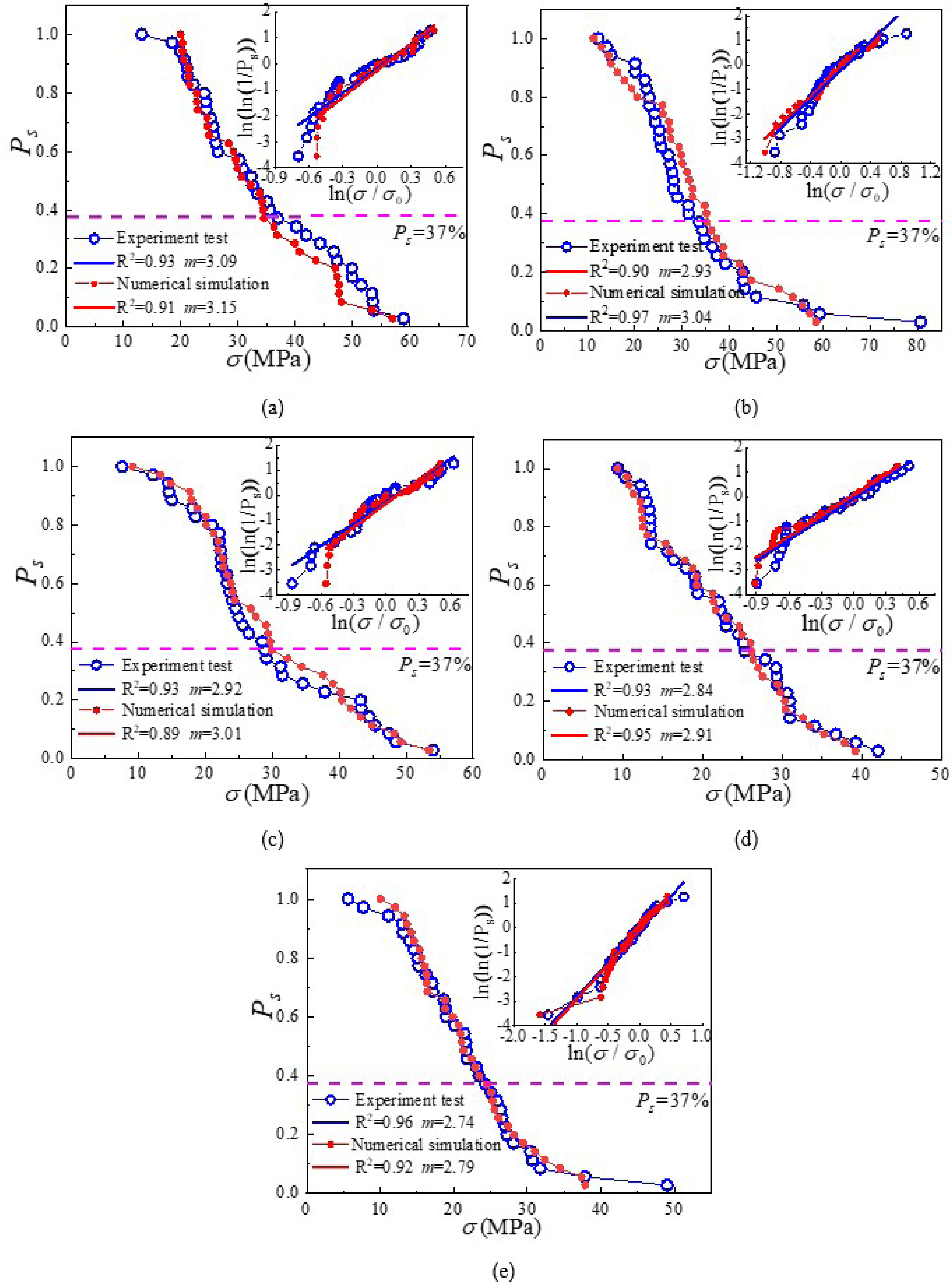


**Figure 8.** Survival probability plot and normalized survival probability plot of experiment test and numerical simulation for different particle sizes: (a) 6-9 mm; (b) 9-12 mm; (c) 12-15 mm; (d) 15-18 mm; (e) 18-21 mm.

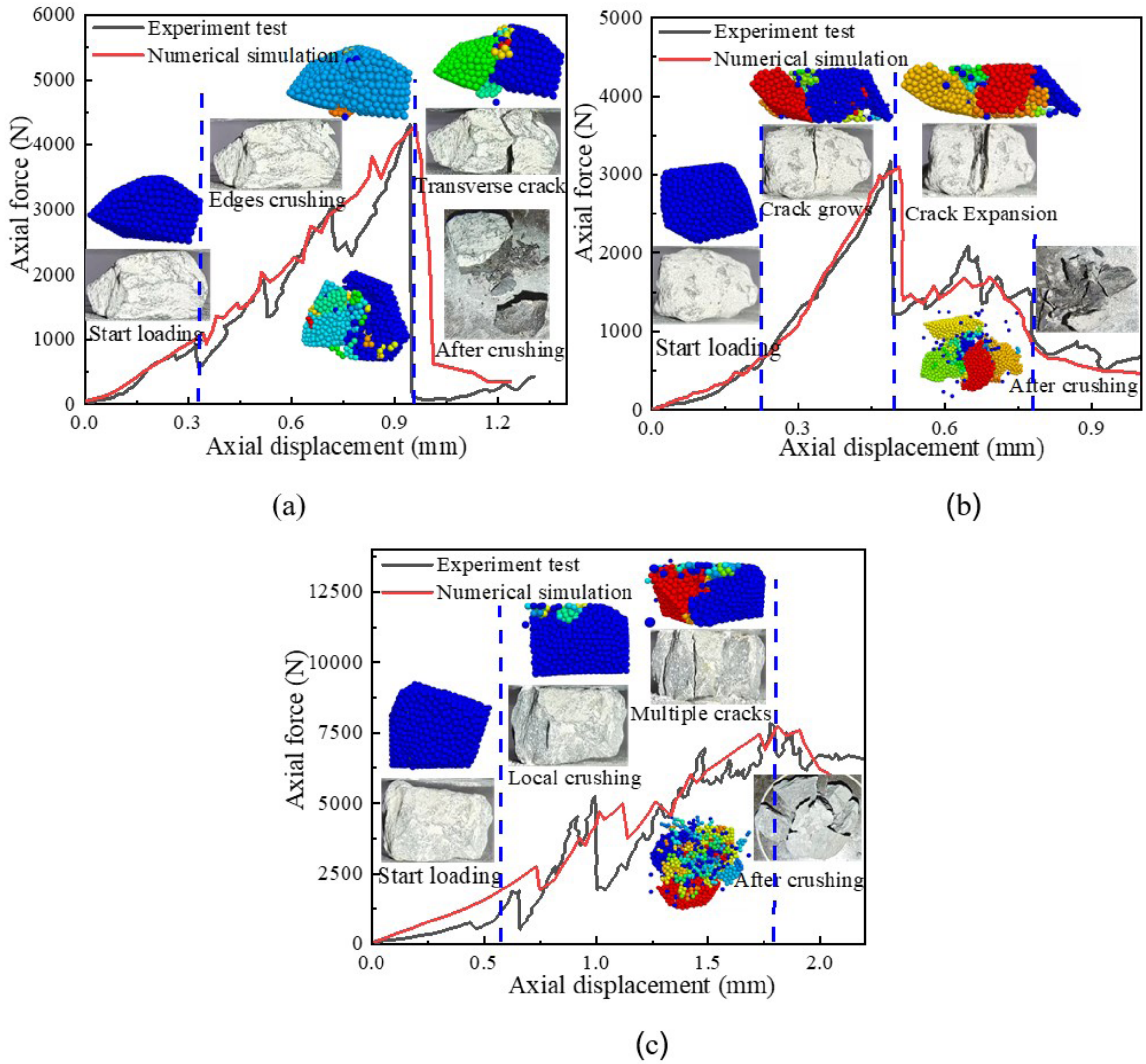


**Figure 9.** Three different crushing modes of rock particles: (a) Mode I; (b) Mode II; (c) Mode III.

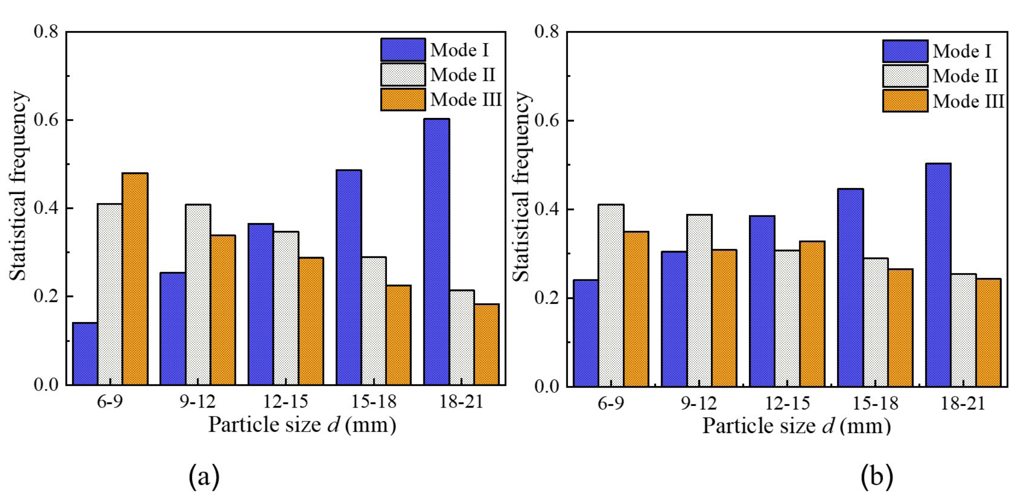


**Figure 10.** Statistical frequency of crushing modes with different particle sizes: (a) experimental results. (b) numerical results.

## 4. Microscopic mechanism of size effect on particle crushing behavior

### 4.1 Microscopic damage characteristic and size correlation of particle crushing

In order to further explore the microscopic mechanism of the size effect of particle crushing behavior, five numerical particles of different size groups were selected. And the changes of the overall damage ratio p, the damage ratio of the weak bonds $p_w$ and the damage ratio of the strong bonds $p_h$ were recorded until the particle reached the peak crushing force. Here, p is defined as the ratio of the number of broken bonds in the compression process to the total number of bonds in the initial particle sample. $p_w$ and $p_h$ are defined as the ratio of the number of weak bonds broken and strong bonds broken in the compression process to the total number of bonds in the initial particle sample, respectively (weak bonds are defined as bonds with bond strength below the Φ; strong bonds are defined as bonds with bond strength above the Φ). For statistical convenience, the bonds of whole numerical particle are only divided into two types of strong and weak bonds.

Figure 11 shows a graph of the variation of p during the compression. The value of the horizontal coordinate corresponding to the dotted line in the diagram is the axial displacement of the particle when it reaches the peak crushing force. From the diagram, p is approximately the same when the peak crushing force is reached for particles of different sizes, about 14%. This means that the overall damage ratio of the internal bonds is the same when the particles of different sizes are broken.

Figure 12 shows the proportion of the damage ratio of strong and weak bonds within the numerical particles of different sizes reach the peak crushing force. From the diagram, when the numerical particles reach the peak crushing force, the damage ratio of the weak bonds $p_w$ are significantly higher than the damage ratio of the strong bonds $p_h$. Defining the bonds damage ratio $\Psi = p_w / p_h$, and count the size of Ψ for numerical particles of different particle sizes, as shown in Figure 13. From the diagram, it can be found that the value of Ψ is increasing as the particle size increases, indicating that the larger the numerical particle size, the weaker bonds will be broken when the peak crushing force is reached.

### 4.2 Microscopic damage function model of particle crushing

For typical brittle rock particles, the damage of failure mode is mainly dominated by axial tensile damage caused by rock intergranular fracture, and the damage surface is usually the middle region of the specimen where the internal tensile stress is larger and parallel to the load direction (Wei et al.,

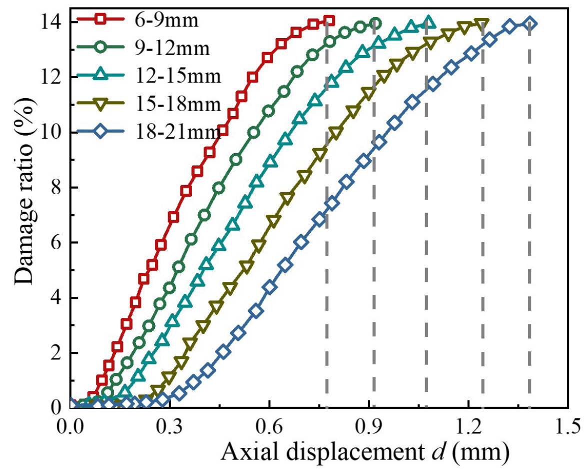


**Figure 11.** Graph of the variation of $p$.

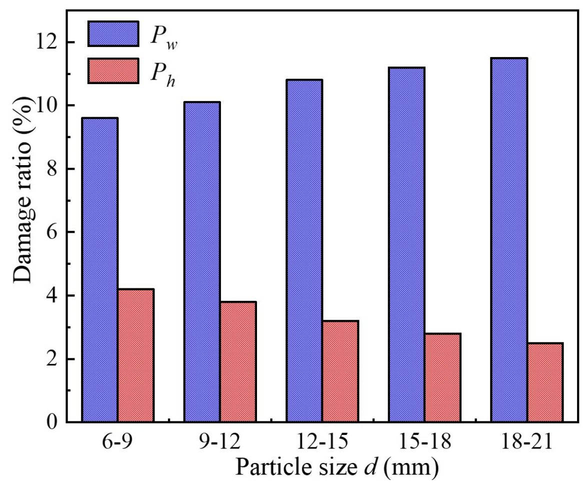


**Figure 12.** Statistics of the $p_w$ and $p_h$.

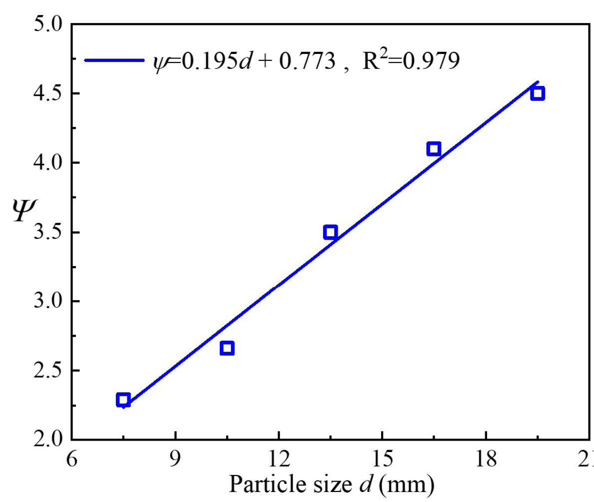


**Figure 13.** Relationship between Ψ and particle sizes $d$.

2022; Ma et al., 2019; Liang et al., 2015; Zhang & Zhao, 2013), which can be simplified by Figure 14.

For the numerical particle crushing test, it can be considered that the particle crushing is mainly caused by the fracture of the bonds in the failure surface. When the particles are broken, it can be considered that the peak crushing force is positively correlated with the number of effective bonds (the number of bonds broken when the particles are damaged by compression), which can be expressed as:

$$F \propto N_e = Np \tag{18}$$

where F represents the peak crushing force of particles, $N_e$ represents the number of effective bonds, N represents the total number of bonds of particles, p represents the overall damage ratio of bonds when the particle reaches the peak crushing force, so $p=p_w+p_h$, then Equation 18 is:

$$F \propto N\left(p_w+p_h\right) \tag{19}$$

Let the $a_w$ and $a_h$ represent the contribution effect of weak and strong bonds to the peak particle crushing force, respectively, and the magnitude of their values is related to the bond failure strength, then we have:

$$F=a_w Np_w + a_h Np_h \tag{20}$$

Transforming the Equation 20 we can get:

$$F=a_w Np(1+\frac{k_1-1}{1+\Psi}) \tag{21}$$

where $k_1=a_h/a_w$, because of $k_1$ represents the ratio of the contribution effect of strong bonds and weak bonds to the peak crushing force of particles, so $k_1>1$. Considering that the failure mode of brittle rock particles is axial tensile failure, so the total number of bonds in the failure surface is positive correlation to the particle diameter, which can be expressed by $N=k_2d^2$. Combining with Equations 14 and 21, the relationship between particle crushing strength σ and bonds damage ratio Ψ can be expressed as:

$$\sigma=\frac{F}{d^2}=a_w k_2 p(1+\frac{k_1-1}{1+\Psi}) \tag{22}$$

For the same kinds of rock particle materials, $a_w, k_2$ and *p* can be considered as constants that do not change with the particle size. So let $a_w k_2 p=k_3$, then the Equation 22 is:

$$\sigma=k_3(1+\frac{k_1-1}{1+\Psi}) \tag{23}$$

The Equation 23 gives the functional relationship between the particle crushing strength and the damage ratio of the strong and weak bonds during the compression crushing process of particles with different sizes. Combining with the numerical test results, the relationship between the particle crushing strength σ and the damage ratio Ψ can be obtained as shown in Figure 15. The result shows that, the Equation 23 can better characterize the relationship between σ and Ψ, its $R^2$ value is 0.98.

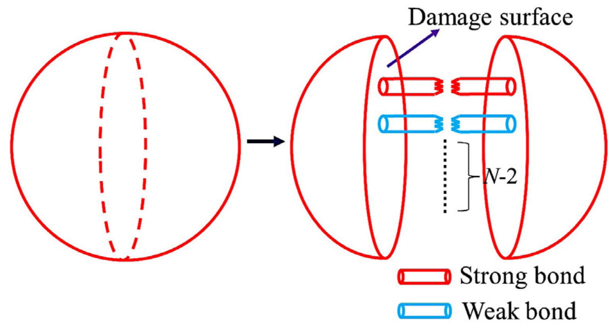


**Figure 14.** Simplified diagram of particle crushing.

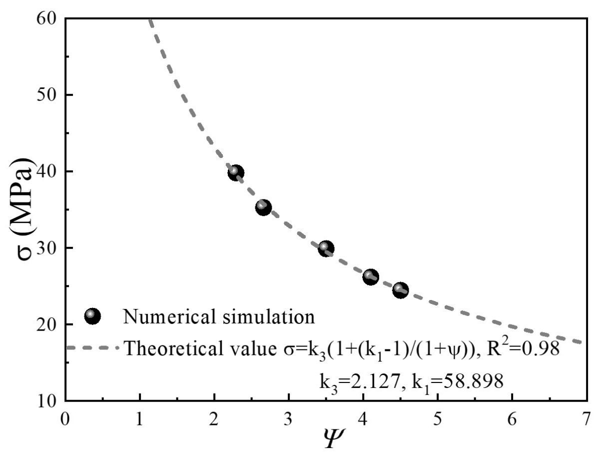


**Figure 15.** Relationship curve between σ and Ψ.

Finally, combined with the results of the Figure 11, Figure 13, and Equation 23, it can be seen that, for different sizes of particles, the overall damage ratio of internal bonds does not change with the change of particle size when the particles are crushed. But with the increase of particle size, the damage ratio of the weak bonds gradually increases, and the damage ratio of the strong bonds gradually decreases when the particles are crushed, which makes the crushing strength of the particles show a size correlation. Showing as the crushing strength of large-size particles is lower than the small-size particles, the crushing strength of the particles show a size effect.

## 5. Conclusions

The uniaxial compression experiments of rock particles with different particle sizes were carried out by experiments and numerical simulation. The main conclusions are as follows:

(1) Based on the discrete element method, a discrete element numerical model considering the characteristics of microscopic heterogeneous bond strength was established. Through the comparison of experiments test and numerical test results, it can be seen that the proposed discrete element numerical model can effectively reproduce the size effect of rock particle crushing behavior;
(2) According to the characteristics of force-displacement curve and particle failure characteristics in the process of rock particle compression, the failure mode of rock particles can be roughly divided into three failure modes. With the increase of particle size, the failure mode gradually changes from "ductile" failure mode to "brittle" failure mode, and the degree of particle crushing is gradually significant;
(3) Based on the numerical test results, a constitutive model between the crushing strength of particles with different sizes and the damage ratio of strong and weak bonds is established, and it is believed that when the particle crushed, the overall damage ratio of bonds inside the particle does not change with the change of the particle size, but the damage ratio of weak bonds inside the particle increase with the increase of the particle size, and the damage ratio of strong bonds decreases with the increase of the particle size. This mechanism makes the particle crushing strength show a significant size correlation, which is manifested in the fact that the crushing strength of large-size particles is lower than that of the small-size particles.

It is worth noting that although the numerical simulation method proposed in this study can to some extent reproduce the size effect characteristics of rock particle fragmentation behavior. However, this method has certain limitations. As the simulated particle size decreases and the number increases, the computational complexity of the numerical model will sharply increase. This not only requires higher computing resources but may also lead to significantly prolonged simulation time. In addition, when dealing with large-scale granular systems, numerical simulations may be limited by computing power and unable to fully reproduce real physical processes. Therefore, in future research, it is necessary to continuously optimize model parameters in order to improve computational efficiency.

## Acknowledgements

This work was supported by the Scientific Research Foundation for Young Scholars of Xiangtan University (No. 21QDZ44), the Natural Science Foundation of Hunan Province, China (No. 2022JJ40440), the Foundation of Hunan Educational Committee (No. 22B0151).

## Declaration of interest

The authors have no conflicts of interest to declare. All co-authors have observed and affirmed the contents of the paper and there is no financial interest to report.

## Authors' contributions

Jiong Qiu: conceptualization, data curation, visualization, writing – original draft. Du-min Kuang: methodology, resources, validation, writing - reviewing and editing. Meng-bo Wang: methodology, investigation, visualization. Long Chen: formal analysis, methodology. Cheng Peng: conceptualization, methodology, validation. Zhao-bo Song: project administration, resources, software.

## Data availability

All data produced or examined in the course of the current study are included in this article.

## Declaration of use of generative artificial intelligence

This work was prepared without the assistance of any generative artificial intelligence (GenAI) tools or services. All aspects of the manuscript were developed solely by the authors, who take full responsibility for the content of this publication.

## List of symbols and abbreviations

| | |
|---|---|
| $a_h$ | The contribution effect of strong bonds to the peak particle crushing force |
| $a_w$ | The contribution effect of weak bonds to the peak particle crushing force |
| $\overline{c}$ | Cohesion |
| $d$ | Particle diameter |
| $d_0$ | Reference particle diameter |
| $i$ | Number of surviving particles at the applied tensile stress |
| $k_1$ | $a_h / a_w$ |
| $k_2$ | $N/d^2$ |
| $k_3$ | $a_w k_2 p$ |
| $\overline{k}_n$ | Normal stiffness |
| $\overline{k}_n / \overline{k}_s$ | Stiffness ratio |
| $\overline{k}_s$ | Shear stiffness |
| $m$ | Weibull modulus |
| $\hat{n}_c$ | Unit-normal vector |
| $p$ | Overall damage ratio |
| $p_h$ | Damage ratio of the strong bonds |
| $p_w$ | Damage ratio of the weak bonds |
| $t$ | A constant value |
| $\overline{A}$ | Cross-sectional area |

| | |
|---|---|
| BPM | Bonded Particle Method |
| DEM | Discrete Element Method |
| $E^*$ | Effective modulus |
| F | Peak force of the particle |
| $\bar{F}$ | Parallel-bond force |
| $\bar{F}_n$ | Normal force |
| $\bar{F}_s$ | Shear force |
| $\bar{I}$ | Polar moment |
| $\bar{J}$ | Moment |
| $\bar{M}$ | Parallel-bond moment |
| $\bar{M}_b$ | Bending moment |
| N | The total number of bonds of particle |
| $\bar{M}_t$ | Twisting moment |
| $N_e$ | The number of effective bonds of particle |
| $N_i$ | Total number of particles |
| $P_s$ | Survival probability |
| $R$ | Rigid radius |
| U | A random value within [0,1] |
| $\beta$ | Damping coefficient |
| $\bar{\beta}$ | Moment-contribution factor |
| $\mu^*$ | Friction coefficient |
| $\rho$ | Density |
| $\sigma$ | Crushing strength of the particle |
| $\bar{\sigma}$ | Tensile stress |
| $\sigma_0$ | Characteristic crushing strength |
| $\bar{\sigma}_c$ | Tensile-strength limit |
| $\bar{\tau}$ | Shear stress |
| $\bar{\tau}_c$ | Shear-strength limit |
| $\varphi$ | Friction angle |
| $\Delta\delta_n$ | Relative normal-displacement increment |
| $\Delta\delta_s$ | Relative shear-displacement increment |
| $\Delta\theta_b$ | Relative bend-rotation increment |
| $\Delta\theta_t$ | Relative twist-rotation increment |
| $\Phi$ | Mean bond strength |
| $\Psi$ | Bonds damage ratio |

## References


Barbosa, L.A.P., Gerke, K.M., Munkholm, L.J., Keller, T., & Gerke, H.H. (2022). Discrete element modeling of aggregate shape and internal structure effects on Weibull distribution of tensile strength. *Soil & Tillage Research*, 219, 105341. http://doi.org/10.1016/j.still.2022.105341.

Chen, H.R., Qin, S.Q., Xue, L., Yang, B.C., Zhang, K., & Wu, X.W. (2017). Characterization of brittle failure of rock and limitation of Weibull distribution. *Progress in Geophysics*, 32(5), 2200-2206. http://doi.org/10.6038/pg20170548.

Cundall, P.A. (1971). A computer model for simulating progressive large-scale movements in blocky rock systems. *International Proceedings Symposium*, 8, 129-136.

Cil, B.M., Sohn, C., & Buscarnera, G. (2020). DEM modeling of grain size effect in brittle granular soils. *Journal of Engineering Mechanics*, 146(3), 04019138. http://doi.org/10.1061/(ASCE)EM.1943-7889.0001713.

Du, X. (2014). Discrete element modeling and optimization of inertial characteristics of real ballast particles. *Journal of Railways*, 36(2), 95-102. http://doi.org/10.3969/j.issn.1001-8360.2014.02.015.

Feng, X.B., Xi, Y., Song, D.Q., & Xu, Y.F. (2016). $PFC^{2D}$ based fractal model for tensile strength and breakage energy of rock particle crushing. *Journal of Engineering Geology*, 24(4), 629-634. http://doi.org/10.13544/j.cnki.jeg.2016.04.019.

Fu, R., Hu, X., & Zhou, B. (2017). Discrete element modeling of crushable sands considering realistic particle shape effect. *Computers and Geotechnics*, 91, 179-191. http://doi.org/10.1016/j.compgeo.2017.07.016.

Guo, X.L., Hu, H., & Bao, C.G. (1997). The effect of particle crushing of rockfill on shear dilation and shear strength. *Journal of Geotechnical Engineering*, (3), 86-91.

Jaeger, J.C. (1967). Failure of rocks under tensile conditions. *International Journal of Rock Mechanics and Mining Sciences & Geomechanics Abstracts*, 4(2), 219-227. http://doi.org/10.1016/0148-9062(67)90046-0.

Jo, S.A., Kim, E.K., Cho, G.C., & Lee, S.W. (2011). Particle shape and crushing effects on direct shear behavior using DEM. *Soil and Foundation*, 51(4), 701-712. http://doi.org/10.3208/sandf.51.701.

Krajcinovic, D., & Silva, M.A.G. (1982). Statistical aspects of me continuous damage theory. *International Journal of Solids and Structures*, 18(7), 551-562. http://doi.org/10.1016/0020-7683(82)90039-7.

Li, X. (1995). *Research and application of post-peak mechanical properties of rock and its damage softening model* (pp. 50-69). Xuzhou: China University of Mining and Technology.

Li, X.F., Li, H.B., Xia, X., Liu, B., & Feng, H.P. (2016). Numerical simulation study on the mechanical properties of direct shear tests of jointed rocks. *Geotechnical Mechanics*, 37(2), 583-591. http://doi.org/10.16285/j.rsm.2016.02.032.

Liang, C.Y., Wu, S.R., Li, X., & Xin, P. (2015). Effects of strain rate on fracture characteristics and mesoscopic failure mechanisms of granite. *International Journal of Rock Mechanics and Mining Sciences*, 76, 146-154. http://doi.org/10.1016/j.ijrmms.2015.03.010.

Matsumoto, M., & Nishimura, T. (1998). Mersenne twister: a 623-dimensionally equidistributed uniform pseudorandom number generator. *ACM Transactions on Modeling and Computer Simulation*, 8(1), 3-30. http://doi.org/10.1145/272991.272995.

Ma, G., Zhou, W., Chang, X.L., & Zhou, C.B. (2011). 3D mesoscopic numerical simulation of triaxial shear tests for rockfill. *Chinese Journal of Geotechnical Engineering*, 33(5), 746-753.

Ma, G., Zhou, W., Regueiro, R.A., Wang, Q., & Chang, X.L. (2017). Modeling the fragmentation of rock grains using computed tomography and combined FDEM. *Powder Technology*, 308, 388-397. http://doi.org/10.1016/j.powtec.2016.11.046.

Ma, L.J., Li, Z., Wang, M.Y., Wei, H.Z., & Fan, P.Y. (2019). Effects of size and loading rate on the mechanical properties of single coral particles. *Powder Technology*, 342, 961-971. http://doi.org/10.1016/j.powtec.2018.10.037.

McDowell, G.R., & Bolton, M.D. (1998). On the micromechanics of crushable aggregates. *Geotechnique*, 48(5), 667-679. http://doi.org/10.1680/geot.1998.48.5.667.

Rabiei, M., Samea, P., Shadi, A., & Ghoreishi-Madiseh, S.A. (2023). A discrete element analysis for general failure behavior of basalt. *International Journal of Rock Mechanics and Mining Sciences*, 167, 105394. http://doi.org/10.1016/j.ijrmms.2023.105394.

Shi, A., Wei, Y., Zhang, Y., & Tang, M. (2020). Study on the strength characteristics of columnar jointed basalt with a true triaxial apparatus at the baihetan hydropower station. *Rock Mechanics and Rock Engineering*, 53(11), 4947-4965. http://doi.org/10.1007/s00603-020-02195-z.

Song, S., Li, S.G., Zhang, T.J., Pan, H.Y., Liu, N., & Zhang, L. (2022). Study on the distribution pattern of particle re-crushing in the coal and rock mass crushing process under pressure. *PLoS One*, 17(1), e0262235. http://doi.org/10.1371/journal.pone.0262235.

Tavares, M.L., & Chagas, D.S.A. (2021). A stochastic particle replacement strategy for simulating breakage in DEM. *Powder Technology*, 377, 222-232. http://doi.org/10.1016/j.powtec.2020.08.091.

Wang, Y.D., Xu, Y.F., & Xi, Y. (2015). Single rock particle crushing in uniaxial compression tests. *Guti Lixue Xuebao*, 36(06), 517-523. http://doi.org/10.19636/j.cnki.cjsm42-1250/o3.2015.06.006.

Wei, H.Z., Ma, L.J., Wu, J.W., Yu, J., Li, Z., & Xu, R. (2022). Dynamic mechanical behavior of coral rock subjected to high strain rate loading. *Marine Geophysical Researches*, 43(3), 30. http://doi.org/10.1007/s11001-022-09493-x.

Xu, W.Y., & Wei, L.D. (2002). Study on statistical damage constitutive model of rock. *Chinese Journal of Rock Mechanics and Engineering*, 21(6), 787-791. http://doi.org/10.3321/j.issn:1000-6915.2002.06.006.

Yokura, K., Yamamoto, H., & Wu, Y. (2015). Crushing tests of soil particles by high pressure true tri-axial compression apparatus. *Japanese Geotechnical Society Special Publication*, 1(2), 51-56. http://doi.org/10.3208/jgssp.JPN-26.

Zhang, Q.B., & Zhao, J. (2013). Effect of loading rate on fracture toughness and failure micromechanisms in marble. *Engineering Fracture Mechanics*, 102, 288-309. http://doi.org/10.1016/j.engfracmech.2013.02.009.

Zhang, T., & Huang, W.X. (2022). DEM analysis of single-particle crushing considering the inhomogeneity of material properties. *Acta Mechanica Solida Sinica*, 35(1), 26-39. http://doi.org/10.1007/s10338-021-00269-1.

Zhang, X., Liu, X., Xu, Y., Wang, G., & Zang, M. (2022). Fragmentation modes of single coral particles under uniaxial compression: microstructural insights. *Construction & Building Materials*, 344, 128186. http://doi.org/10.1016/j.conbuildmat.2022.128186.

Zhang, Y.H., Zhou, H.M., & Zhong, Z.W. (2011). YXSW-12 in-situ rock mass true triaxial testing system and its application. *Journal of Rock Mechanics and Engineering*, 30(11), 2312-2320. Retrieved in September 9, 2023, from https://cnki:sun:yslx.0.2011-11-018

Zhao, T., & Liu, Y. (2020). A novel random discrete element analysis of rock fragmentation. *International Journal for Numerical and Analytical Methods in Geomechanics*, 44(10), 1386-1395. http://doi.org/10.1002/nag.3067.

Zheng, W.B., Hu, X.L., Tannant, D.D., Zhang, K., & Xu, C. (2019). Characterization of two-and three-dimensional morphological properties of fragmented sand grains. *Engineering Geology*, 263, 105358. http://doi.org/10.1016/j.enggeo.2019.105358.

Zhou, M.J., Wen, Y.F., Deng, G., Wang, Y.J., & Song, E.X. (2019). Three-dimensional discrete element simulation of random breaking strength and size effect in single particle splitting test of rockfill. *Yantu Lixue*, 40(S1), 503-510. http://doi.org/10.16285/j.rsm.2018.1678.

Zhou, H.J., Ma, G., Yuan, W., Zhou, W., & Chang, X.L. (2017). Size effect on the crushing strengths of rock particles. *Yantu Lixue*, 38(08), 2425-2433. http://doi.org/10.16285/j.rsm.2017.08.032.

Zhou, W., Chang, X.L., Zhou, C.B., & Zhu, K.X. (2009). Stochastic granule discontinuous deformation model of rockfill and its application. *Chinese Journal of Rock Mechanics and Engineering*, 28(3), 491-499. http://doi.org/10.3321/j.issn:1000-6915.2009.03.007.

Zhu, D.J., Yang, L.D., & Cai, Y.C. (2009). Research on the anisotropy characteristics and size effects of columnar jointed rock masses. *Journal of Rock Mechanics and Engineering*, 28(7), 1405-1414. http://doi.org/10.3321/j.issn:1000-6915.2009.07.014.